

# Continuum quasiparticle linear response theory using the Skyrme functional for multipole responses of exotic nuclei

Kazuhito Mizuyama,<sup>1,\*</sup> Masayuki Matsuo,<sup>2</sup> and Yasuyoshi Serizawa<sup>1</sup>

<sup>1</sup>*Graduate School of Science and Technology, Niigata University, Niigata 950-2181, Japan*

<sup>2</sup>*Department of Physics, Faculty of Science, Niigata University, Niigata 950-2181, Japan*

(Dated: October 30, 2018)

We develop a new formulation of the continuum quasiparticle random phase approximation (QRPA) in which the velocity dependent terms of the Skyrme effective interaction are explicitly treated except the spin dependent and the Coulomb terms. Numerical analysis using the SkM\* parameter set is performed for the isovector dipole and the isovector/isoscalar quadrupole responses in <sup>20</sup>O and <sup>54</sup>Ca. It is shown that the energy-weighted sum rule including the enhancement factors for the isovector responses is satisfied with good accuracy. We investigate also how the velocity dependent terms influence the strength distribution and the transition densities of the low-lying surface modes and the giant resonances.

PACS numbers: 21.10.Pc, 21.10.Re, 21.60.Jz, 24.30.Cz

## I. INTRODUCTION

Nuclei near the neutron drip-line provide us with many new physics issues which arise from the presence of weakly bound neutrons and the coupling to unbound neutron states. The ground state and the excitation modes of a near-drip-line nucleus are indeed very different from those of stable nuclei as is testified by the observations of the neutron halo[1], the neutron skin[2] and the soft dipole excitation[3]. In addition the nucleon correlations such as the pairing may also be influenced in the new circumstances[4, 5]. Consequently there has been considerable efforts in the last two decades to develop nuclear many-body theories toward this direction.

Focusing on near-drip-line nuclei in the medium mass region, theoretical approaches based on the self-consistent mean-field methods or the density functional theories are of great promise. The Hartree-Fock-Bogoliubov (HFB) theory [6], especially those employing the coordinate-space representation [4, 5, 7], has been playing a central role to describe the ground state and the pair correlation. The HFB theory provides us also with the basis for further theoretical developments to describe the dynamics, e.g. the excitation modes built on the ground state. Indeed new schemes of the quasiparticle random phase approximations (QRPA) formulated on the basis of the coordinate-space HFB have been recently proposed and applied extensively to studies of multipole responses of unstable nuclei [8, 9, 10, 11, 12, 13, 14, 15, 16, 17, 18, 19, 20, 21, 22, 23, 24, 25] (see also references in Ref.[26]).

There are two important requirements to be considered when the HFB+QRPA theories are applied to near-drip-line nuclei. First of all, the coupling of excitation modes to the continuum states have to be taken into account

since most of excitation modes including even the low-lying excitations are located near or above the nucleon separation energy. This can be achieved by means of the continuum QRPA methods [10, 11, 12, 13, 14, 15]. Secondly, the QRPA description should be consistent with the HFB description of the ground state in the sense that the same effective interaction or the same density functional should be used for both descriptions. If this is achieved, one can calculate the ground and excited states solely from the effective interaction (or the energy density functional) without relying on phenomenological parameterization of the mean-fields. This is often called the requirement of the self-consistency. The two requirements, however, have been in a trade-off relation in the actual implementations. Namely in the continuum QRPA methods which fulfill the first requirement the self-consistency has been left behind since the residual interaction for the QRPA description is often approximated to a tractable simple contact force[10, 11, 12] or the Landau-Migdal forces [13, 14, 15]. On the other hand, recently developed fully self-consistent QRPA's using the Skyrme functional[23, 24] and the relativistic mean-field functional[18, 19] treat approximately the continuum states by employing the finite-box discretization or the discrete oscillator basis.

It is therefore important to develop a new formulation of the continuum QRPA which is based on the nuclear density functional and thus satisfies the self-consistency as precisely as possible. In the present paper we try to make a one step progress in this direction.

To this end we shall proceed in the following way. We start with the Skyrme's Hartree-Fock energy functional combined with the pair correlation energy. We then use this functional not only for the static Hartree-Fock-Bogoliubov mean-fields but also to derive the residual interaction to be used in the continuum QRPA. In formulating the new continuum QRPA, we pay special attention to the energy weighted sum rule, which is not satisfied in the previous continuum QRPA's [10, 11, 12, 13, 14, 15]. To satisfy this we take into account explicitly

---

\*Electronic address: mizu@nt.sc.niigata-u.ac.jp

the velocity dependent central terms of the Skyrme effective interaction to derive the residual interaction, and then implement the residual interaction into the Green's function formulation of the continuum QRPA proposed in Ref.[10]. In the present paper, however, we do not include the spin dependent densities and the Coulomb interaction in deriving the residual interaction, and hence the goal of the full self-consistency is not achieved yet. Our formulation of the Skyrme QRPA is similar to that of Ref.[20, 21] apart from the treatments of the continuum quasiparticle states, on which we impose the outgoing wave boundary condition instead of the finite-box discretization.

By performing numerical calculations, we shall demonstrate that the Skyrme continuum QRPA in the present formulation indeed satisfies the sum rule as far as the dipole and quadrupole responses with natural parities are concerned. We shall also show that the inclusion of the velocity dependent terms gives better description of the strength function and the transition densities of the multipole responses in comparison with the previous continuum QRPA that utilizes residual interactions of the simple contact forces.

The paper is organized as follows. The formulation is given in the next section. In Section III we present results of numerical calculation performed for the isovector dipole and the isoscalar/isovector quadrupole responses in neutron-rich O and Ca isotopes. We discuss both the low-lying excitations and the giant resonances. We shall illustrate in detail the importance of taking account of the velocity dependent terms by comparing with the Landau-Migdal approximation of the Skyrme effective interaction[27, 28]. The conclusions are drawn in Section IV.

## II. CONTINUUM QRPA USING THE SKYRME FUNCTIONAL

In this section, we give a formulation of the continuum QRPA which is based on the Skyrme functional.

We start with the energy functional of the system defined for a determinantal many-body state vector  $|\Phi(t)\rangle$  of the generalized form in which the pair correlation is taken into account by means of the Bogoliubov's quasiparticle method[6]. The time-dependence is explicitly written here since we consider dynamical multipole responses of the system under a time-dependent perturbation. The energy functional  $E = E_{Skyrme} + E_{pair}$  consists of the Skyrme Hartree-Fock energy  $E_{Skyrme}$  and the pair correlation energy  $E_{pair}$ . The Skyrme Hartree-Fock energy  $E_{Skyrme}$  is expressed in terms of the local density  $\rho_q(\mathbf{r}, t)$ , its spatial derivatives  $\nabla\rho_q(\mathbf{r}, t)$  and  $\Delta\rho_q(\mathbf{r}, t)$ , the current density  $\mathbf{j}_q(\mathbf{r}, t)$ , the kinetic energy density  $\tau_q(\mathbf{r}, t)$ , the spin density  $\mathbf{s}_q(\mathbf{r}, t)$  and the spin-orbit tensor  $\mathbf{J}_q(\mathbf{r}, t)$  where  $q = n, p$  stands for the neutron or proton components[29, 30]. Given a parameter set such as SIII[31], SkM\*[32] and SLy4[33], the Skyrme Hartree-

Fock energy functional  $E_{Skyrme}[\rho, \nabla\rho, \Delta\rho, \tau, \mathbf{j}, \mathbf{s}, \mathbf{J}]$  is completely specified. Concerning the pair correlation energy  $E_{pair}$ , we use the one evaluated for the density-dependent delta interaction (DDDI) [34, 35]

$$V_{pair}(1, 2) = \frac{1}{2}V_0(1 - P_\sigma) \left[ 1 - \eta \left( \frac{\rho(\mathbf{r})}{\rho_c} \right)^\gamma \right] \delta(\mathbf{r} - \mathbf{r}'). \quad (1)$$

$E_{pair}$  is a functional of the local density  $\rho_q(\mathbf{r}, t)$  and the local pair densities

$$\tilde{\rho}_{\pm q}(\mathbf{r}, t) = \langle \Phi(t) | \psi_q^\dagger(\mathbf{r} \downarrow) \psi_q^\dagger(\mathbf{r} \uparrow) \pm \psi_q(\mathbf{r} \uparrow) \psi_q(\mathbf{r} \downarrow) | \Phi(t) \rangle. \quad (2)$$

Application of the static variational principle to the total energy functional  $E_{Skyrme} + E_{pair}$  leads to the Hartree-Fock-Bogoliubov equation

$$\mathcal{H}_{0q} \phi_q(\mathbf{r}\sigma) = E_q \phi_q(\mathbf{r}\sigma) \quad (3)$$

for the quasiparticle wave function

$$\phi_q(\mathbf{r}\sigma) = \begin{pmatrix} \varphi_{q,1}(\mathbf{r}\sigma) \\ \varphi_{q,2}(\mathbf{r}\sigma) \end{pmatrix}. \quad (4)$$

Here

$$\mathcal{H}_{0q} = \begin{pmatrix} h_q - \lambda_q & \tilde{h}_q \\ \tilde{h}_q^* & -h_q^* + \lambda_q \end{pmatrix} \quad (5)$$

is the  $2 \times 2$  matrix representation of the HFB mean-field Hamiltonian

$$\begin{aligned} \hat{h} &= \sum_q \int d\mathbf{r} d\mathbf{r}' \sum_{\sigma, \sigma'} h_q(\mathbf{r}\sigma, \mathbf{r}'\sigma') \psi_q^\dagger(\mathbf{r}\sigma) \psi_q(\mathbf{r}'\sigma') \\ &+ \frac{1}{2} \int d\mathbf{r} d\mathbf{r}' \sum_{\sigma, \sigma'} \tilde{h}_q(\mathbf{r}\sigma, \mathbf{r}'\tilde{\sigma}') \psi_q^\dagger(\mathbf{r}\sigma) \psi_q^\dagger(\mathbf{r}'\tilde{\sigma}') \\ &+ h.c. \end{aligned} \quad (6)$$

The Hartree-Fock Hamiltonian  $h_q$  and the pair potential  $\tilde{h}_q$  are defined through the functional derivative of the energy functionals  $E_{Skyrme}$  and  $E_{pair}$ , respectively.

We consider multipole response of the nucleus under a small time-dependent external perturbation

$$\begin{aligned} \hat{V}_{ext}(t) &= e^{-i\omega t} \sum_q \int d\mathbf{r} f_q(\mathbf{r}) \sum_\sigma \psi_q^\dagger(\mathbf{r}\sigma) \psi_q(\mathbf{r}\sigma) \\ &+ h.c. \end{aligned} \quad (7)$$

expressed in terms of a one-body spin-independent local field  $f_q(\mathbf{r})$ , for which we take a multipole field  $\propto r^L Y_{LM}$  such as the electric dipole and the isoscalar/isovector quadrupole fields.

The external perturbation causes the induced fields in the Hartree-Fock mean-field and the pair potential, which we denote  $\delta h_q$  and  $\delta \tilde{h}_q$ , respectively.  $\delta h_q$  and  $\delta \tilde{h}_q$  are expressed in terms of fluctuations in the various one-body densities

$$\begin{aligned} &\delta\rho_q(\mathbf{r}, t), \delta\nabla\rho_q(\mathbf{r}, t), \delta\Delta\rho_q(\mathbf{r}, t), \delta\tau_q(\mathbf{r}, t), \delta\mathbf{j}_q(\mathbf{r}, t), \\ &\delta\mathbf{J}_q(\mathbf{r}, t), \delta\mathbf{s}_q(\mathbf{r}, t), \\ &\delta\tilde{\rho}_{\pm q}(\mathbf{r}, t) \end{aligned} \quad (8)$$

and the second derivatives of the energy functional. A fully self-consistent QRPA based on the Skyrme HFB functional can be constructed if one considers all the kinds of density fluctuations in Eq.(8). In the previous continuum QRPA approaches, however, only the fluctuations in the local densities  $\delta\rho_q(\mathbf{r}, t)$  and  $\delta\tilde{\rho}_{\pm q}(\mathbf{r}, t)$ , and the induced fields associated with these density fluctuations have been taken into account [10, 11, 12, 13, 14, 15]. Although this approximation has a large number of practical usefulness, it is not sufficient in some respects: it violates the energy weighted sum rule when the Skyrme HF mean-field with the effective mass is adopted. This is because the current conservation law is not satisfied when the velocity dependent parts (the terms proportional to the  $t_1$  and  $t_2$  terms) of the Skyrme interaction and the current fluctuations  $\delta\mathbf{j}_q$  are neglected in the RPA[36, 37, 38, 39]. We aim at improving this point. For this purpose we shall include all the density fluctuations that are responsible for the energy weighted sum rule for the responses caused by the spin independent local multipole fields. They are the fluctuations  $\delta\mathbf{j}_q$ ,  $\delta\nabla\rho_q$ ,  $\delta\Delta\rho_q$ , and  $\delta\tau_q$  in the current, the spatial derivatives of the density and the kinetic energy density. It is more preferable to take into account also the fluctuations in the spin-dependent densities  $\mathbf{s}_q$  and  $\mathbf{J}_q$ , but we neglect them in the present work. This is one approximation which remains in the present approach. We neglect the residual Coulomb interaction. The cross derivatives among  $\rho_q$  and  $\tilde{\rho}_{\pm q}$  are also neglected. These are the second approximation we introduce. Consequently the full self-consistency is not fulfilled, but the treatment of the residual interaction is significantly improved compared to the previous continuum QRPA approaches [10, 11, 12, 13, 14, 15] in the sense that the present formalism allows us to describe the correct energy weighted sum rule for the multipole responses. Note also that the approximate treatment of the particle-hole residual interaction is comparable to that adopted in the currently available continuum RPA approaches which utilize the Skyrme-Hartree-Fock functional without taking into the pairing [40, 41, 42, 43]. On the other hand, we should keep in mind that the approximation neglecting the spin dependent densities may not be justified for multipole responses with unnatural parities involving spin excitations.

The induced fields under the above approximations are expressed as

$$\delta h_q = \sum_{q'} a_{qq'} \delta\rho_{q'} + b_{qq'} \delta\Delta_+\rho_{q'} + \left[ \overleftarrow{\Delta} + \overrightarrow{\Delta} \right] b_{qq'} \delta\rho_{q'}$$

in the frequency domain.

Here  $R_{0q}^{\alpha\beta}(\mathbf{r}\mathbf{r}', \omega)$  is the unperturbed response function

$$+ \left[ \overleftarrow{\nabla} + \overrightarrow{\nabla} \right] \cdot c_{qq'} \delta\nabla\rho_{q'} + \left[ \overleftarrow{\nabla} - \overrightarrow{\nabla} \right] \cdot b_{qq'} \delta 2i\mathbf{j}_{q'} \quad (9)$$

and

$$\delta\tilde{h}_q = \tilde{a}_q \delta\tilde{\rho}_{+q} - \tilde{a}_q \delta\tilde{\rho}_{-q}. \quad (10)$$

The functions  $a_{qq'}$ ,  $b_{qq'}$ ,  $c_{qq'}$  and  $\tilde{a}_q$  are expressed in terms of the local densities and the effective interaction parameters. The definition of  $a_{qq'}$ ,  $b_{qq'}$  and  $c_{qq'}$  follows Ref. [43], and their detailed expressions are given in Appendix. Note here that we use  $\delta\Delta_+\rho_q(\mathbf{r}, t) \equiv (\Delta + \Delta')\delta\rho_q(\mathbf{r}\mathbf{r}', t)|_{\mathbf{r}'=\mathbf{r}} = \delta\Delta\rho_q(\mathbf{r}, t) - 2\delta\tau_q(\mathbf{r}, t)$  in place of  $\delta\Delta\rho_q(\mathbf{r}, t)$ , where  $\rho_q(\mathbf{r}\mathbf{r}', t)$  is the density matrix. We also attached a factor  $2i$  to the current fluctuation  $\delta\mathbf{j}_q$  so that  $\delta 2i\mathbf{j}_q = (\nabla - \nabla')\delta\rho_q(\mathbf{r}\mathbf{r}', t)|_{\mathbf{r}'=\mathbf{r}}$  becomes in parallel with  $\delta\nabla\rho_q = (\nabla + \nabla')\delta\rho_q(\mathbf{r}\mathbf{r}', t)|_{\mathbf{r}'=\mathbf{r}}$ . The fluctuation in the kinetic energy density  $\delta\tau_q(\mathbf{r}, t)$  does not appear here since it can be eliminated from the induced field by a partial integration. Nevertheless we eventually include  $\delta\tau_q$  as explained later.

The induced fields are also represented in the  $2 \times 2$  matrix form as

$$\begin{pmatrix} \delta h_q & \delta\tilde{h}_q \\ \delta h_q^* & -\delta\tilde{h}_q^* \end{pmatrix} = \sum_{\beta} \mathcal{B}^{\beta} \hat{O}^{\beta} \sum_{\gamma} \kappa_{\beta\gamma} \delta\rho_{\gamma} \quad (11)$$

where  $\delta\rho_{\gamma}$  is a collective notation for

$$\delta\rho_{\gamma} \in \delta\rho_q, \delta\Delta_+\rho_q, \delta\nabla\rho_q, \delta 2i\mathbf{j}_q, \delta\tilde{\rho}_{\pm q}. \quad (12)$$

and  $\hat{O}^{\beta}$  denotes the derivative operators  $1, \overleftarrow{\Delta} + \overrightarrow{\Delta}, \overleftarrow{\nabla} - \overrightarrow{\nabla}$  and  $\overleftarrow{\nabla} + \overrightarrow{\nabla}$  while  $\mathcal{B}^{\beta}$  stands for one of the  $2 \times 2$  matrices  $\begin{pmatrix} 1 & 0 \\ 0 & -1 \end{pmatrix}, \begin{pmatrix} 1 & 0 \\ 0 & 1 \end{pmatrix}, \begin{pmatrix} 0 & 1 \\ 1 & 0 \end{pmatrix}$  and  $\begin{pmatrix} 0 & 1 \\ -1 & 0 \end{pmatrix}$ .  $\kappa_{\beta\alpha}$  represents the functions  $a_{qq'}$ ,  $b_{qq'}$ ,  $c_{qq'}$  and  $\tilde{a}_q$  in Eqs.(9) and (10). The correspondence among  $\hat{O}^{\alpha}$ ,  $\mathcal{B}^{\alpha}$ ,  $\kappa_{\beta\gamma}$  and  $\delta\rho_{\gamma}$  is shown in Table I.

The external perturbation and the induced fields cause quasi-particle excitations, which in turn bring about fluctuations in the densities  $\delta\rho_q$ ,  $\delta\tilde{\rho}_{\pm q}$ ,  $\delta\Delta_+\rho_q$ ,  $\nabla\delta\rho_q$  and  $\delta 2i\mathbf{j}_q$ . This relation is given by the linear response equation, which is written as

$$\delta\rho_{\alpha}(\mathbf{r}, \omega) = \sum_{\beta} \int d\mathbf{r}' R_{0q}^{\alpha\beta}(\mathbf{r}\mathbf{r}', \omega) \left[ \sum_{\gamma} \kappa_{\beta\gamma}(\mathbf{r}') \delta\rho_{\gamma}(\mathbf{r}', \omega) + \delta_{\beta,0q} f_q(\mathbf{r}) \right] \quad (13)$$

for the density  $\delta\rho_{\alpha}$  and the field  $\mathcal{B}^{\beta} \hat{O}^{\beta}$ . Using the Green's

function formalism of the continuum QRPA[10], the unperturbed response function is expressed as

$$R_{0q}^{\alpha\beta}(\mathbf{r}\mathbf{r}', \omega) = \frac{1}{4\pi i} \int_C dE \text{Tr} \left[ \mathcal{A}^\alpha \hat{O}^\alpha(\mathbf{r}) \mathcal{G}_{0q}(\mathbf{r}\mathbf{r}', E + \hbar\omega + i\epsilon) \mathcal{B}^\beta \hat{O}^\beta(\mathbf{r}') \mathcal{G}_{0q}(\mathbf{r}'\mathbf{r}, E) \right] + \frac{1}{4\pi i} \int_C dE \text{Tr} \left[ \mathcal{A}^\alpha \hat{O}^\alpha(\mathbf{r}) \mathcal{G}_{0q}(\mathbf{r}\mathbf{r}', E) \mathcal{B}^\beta \hat{O}^\beta(\mathbf{r}') \mathcal{G}_{0q}(\mathbf{r}'\mathbf{r}, E - \hbar\omega - i\epsilon) \right] \quad (14)$$

in terms of the quasi-particle Green's function  $\mathcal{G}_{0q}(E) = (E - \mathcal{H}_{0q})^{-1}$  and a contour integral in the complex energy plane. The complex energy integral is performed on a rectangular contour  $C$  enclosing the negative energy part of the real  $E$  axis with the two sides located at  $\pm \frac{i}{2}\epsilon$  [10]. Here  $\epsilon$  is a small parameter which plays a role of the smoothing energy width. The matrices  $\mathcal{A}^\alpha$  and  $\mathcal{B}^\beta$  and the operators  $\hat{O}^\alpha$  and  $\hat{O}^\beta$  follow Table I, but we remark that the matrix  $\mathcal{A}^\alpha$  takes a form  $\mathcal{A}^\alpha = \begin{pmatrix} 2 & 0 \\ 0 & 0 \end{pmatrix}$  for the particle-hole densities  $\delta\rho_q, \delta\Delta_+\rho_q, \delta\nabla\rho_q, \delta 2i\mathbf{j}_q$  and  $\delta\tau_q$  while the matrix  $\mathcal{B}^\beta$  has the following definitions:  $\mathcal{B}^\beta = \begin{pmatrix} 1 & 0 \\ 0 & -1 \end{pmatrix}$  for the 'time-even' quantities  $\delta\rho_q, \delta\Delta_+\rho_q$  and  $\delta\nabla\rho_q$ , and  $\mathcal{B}^\beta = \begin{pmatrix} 1 & 0 \\ 0 & 1 \end{pmatrix}$  for the 'time-odd'  $\delta 2i\mathbf{j}_q$  (See Table I).

Let us assume the spherical symmetry of the ground state, and we apply the multipole decompositions. Let  $L$  be the multipolarity of the excitation modes under consideration. The fluctuation in the scalar quantities  $\delta\rho_\alpha = \delta\rho_q, \delta\tilde{\rho}_{\pm q}$  and  $\delta\Delta_+\rho_q$  are expanded as

$$\delta\rho_\alpha(\mathbf{r}, \omega) = Y_{LM}(\hat{\mathbf{r}}) [\delta\rho_\alpha]_L / r^2, \quad (15)$$

and we now consider only the radial functions  $[\delta\rho_\alpha]_L = [\delta\rho_q]_L, [\delta\tilde{\rho}_{\pm q}]_L$  and  $[\delta\Delta_+\rho_q]_L$ . Concerning the vector

quantities  $\delta\rho_\alpha = \delta\nabla\rho_q$  and  $\delta 2i\mathbf{j}_q$ , they are expanded as

$$\delta\rho_\alpha(\mathbf{r}, \omega) = \sum_{\lambda=L\pm 1} \mathbf{Y}_{L\lambda M}(\hat{\mathbf{r}}) [\delta\rho_\alpha]_L^\lambda / r^2, \quad (16)$$

in terms of the vector spherical harmonics  $\mathbf{Y}_{L\lambda M}$  and the radial functions  $[\delta\rho_\alpha]_L^\lambda = [\delta\nabla\rho_q]_L^{\lambda=L\pm 1}$  and  $[\delta 2i\mathbf{j}_q]_L^{\lambda=L\pm 1}$ . Note that only the terms  $\lambda = L \pm 1$  remain here since we consider the multipole excitations with the natural parity. Then the linear response equation (13) is rewritten as an equation for the relevant radial functions  $[\delta\rho_q]_L, [\delta\tilde{\rho}_{\pm q}]_L, [\delta\Delta_+\rho_q]_L, [\delta\nabla\rho_q]_L^{\lambda=L\pm 1}$  and  $[\delta 2i\mathbf{j}_q]_L^{\lambda=L\pm 1}$ . Denoting collectively these density fluctuations  $\delta\rho_{\alpha L}$ , the linear response equation for these variables is given by

$$\begin{aligned} & \delta\rho_{\alpha L}(r, \omega) \\ &= \sum_\beta \int dr' R_{0,qL}^{\alpha\beta}(rr'\omega) \\ & \quad \times \left[ \sum_\gamma \kappa_{\beta\gamma} \delta\rho_{\gamma L}(r', \omega) / r'^2 + \delta_{\beta,0q} f_{qL}(r') \right] \end{aligned} \quad (17)$$

using the unperturbed response function for the fixed multipolarity  $L$

$$\begin{aligned} & R_{0,qL}^{\alpha\beta}(rr', \omega) \\ &= \frac{1}{4\pi i} \int_C dE \sum_{l'j'l_j} \frac{|\langle l'j' || Y_L || lj \rangle|^2}{2L+1} \text{Tr} \left[ \mathcal{A}^\alpha \hat{O}_{l'j'l_j}^\alpha(r) \mathcal{G}_{0,q'l'j'}(rr', E + \hbar\omega + i\epsilon) \mathcal{B}^\beta \hat{O}_{l'j'l_j}^\beta(r') \mathcal{G}_{0,q'l_j}(r'r, E) \right] \\ & \quad + \text{Tr} \left[ \mathcal{A}^\alpha \hat{O}_{l'j'l_j}^\alpha(r) \mathcal{G}_{0,q'l_j}(rr', E) \mathcal{B}^\beta \hat{O}_{l'j'l_j}^\beta(r') \mathcal{G}_{0,q'l'j'}(r'r, E - \hbar\omega - i\epsilon) \right]. \end{aligned} \quad (18)$$

Here  $\mathcal{G}_{0,q'l_j}(r'r, E)$  is the  $2 \times 2$  radial HFB Green's function for specified orbital and total angular momenta  $l$  and  $j$ , and  $\hat{O}_{l'j'l_j}^\beta$  is the radial derivative operator cor-

responding to the previously defined  $\hat{O}^\beta$ . Their explicit forms are given in Table I. We adopt the exact form for the radial HFB Green's function[44] constructed as

$$\mathcal{G}_{0,qlj}(rr', E) = \sum_{s,s'=1,2} c_{qlj}^{ss'}(E) \left( \theta(r-r') \phi_{qlj}^{(+s)}(r, E) \phi_{qlj}^{(rs')T}(r', E) + \theta(r'-r) \phi_{qlj}^{(rs')}(r, E) \phi_{qlj}^{(+s)T}(r', E) \right) \quad (19)$$

in terms of two independent solutions  $\phi_{qlj}^{(rs)}(r, E)$  ( $s = 1, 2$ ) regular at the origin  $r = 0$  of the radial HFB equation and two independent solutions  $\phi_{qlj}^{(+s)}(r, E)$  ( $s = 1, 2$ ) satisfying the out-going boundary condition. (The construction (19) is the same as that used in Refs.[10, 44] except that the effective mass should be taken into account in the definitions of the Wronskian and the coefficients  $c_{qlj}^{ss'}$  while in Refs.[10, 44] the bare mass is assumed.). In this way the exact treatment of the continuum single-particle states satisfying the proper boundary condition is implemented in the QRPA formalism.

Note that in Table I we use the following convention for the derivative operators marked with the right/left-sided arrows such as  $\overrightarrow{\partial} \pm \overleftarrow{\partial}$ . When this derivative is inserted in  $\hat{O}_{l'j'l_j}^\beta(r')$  in the first term of r.h.s. of Eq.(18), the derivative symbol  $\overrightarrow{\partial}$  with the right-sided arrow indicates that it acts on the coordinate  $r'$  in the Green's function  $\mathcal{G}_{0,qlj}(r'r, E)$  while the other one  $\overleftarrow{\partial}$  with the left-sided arrow acts on the Green's function  $\mathcal{G}_{0,ql'j'}(rr', E + \hbar\omega + i\epsilon)$ . The same rule is applied also to the operator  $\hat{O}_{l'j'l_j}^\alpha(r)$ , i.e.,  $\overrightarrow{\partial}$  acts on  $r$  in  $\mathcal{G}_{0,ql'j'}(rr', E + \hbar\omega + i\epsilon)$  while  $\overleftarrow{\partial}$  on  $r$  in  $\mathcal{G}_{0,qlj}(r'r, E)$ . The ordering of the operators and the Green's functions

makes sense in Eq.(18).

To obtain a numerical solution of the linear response equation, we need to rewrite further Eq.(17). When the radial derivative operators  $\frac{\partial}{\partial r}$  and  $\frac{\partial}{\partial r'}$  act on the radial HFB Green's function like  $\overrightarrow{\partial} \mathcal{G}_{0,qlj}(rr', E) \overleftarrow{\partial}$ , a singular term proportional to  $\frac{2m_q^*(r)}{\hbar^2} \delta(r-r')$  emerges. We need to treat these singular terms separately in the numerical calculation. For this purpose we rewrite the derivative of the Green's function into singular and regular parts

$$\overrightarrow{\partial} \mathcal{G}_{0,qlj}(rr', E) \overleftarrow{\partial} = -\frac{2m_q^*(r)}{\hbar^2} \delta(r-r') + \overrightarrow{\partial} \mathcal{G}_{0,qlj}(rr', E) \overleftarrow{\partial} \quad (20)$$

where the regular part (the second term in r.h.s denoted with the tilded derivatives) is defined as a part of  $\overrightarrow{\partial} \mathcal{G}_{0,qlj}(rr', E) \overleftarrow{\partial}$  that arises from the action of the derivatives on the wave functions  $\phi_{l_j}^{(rs)}$  and  $\phi_{l_j}^{(+s)}$  in Eq.(19), but not on the Heaviside theta function  $\theta(r-r')$ . Inserting this decomposition into the response function(Eq.(18)), the r.h.s. of the linear response equation (17) is decomposed into two parts:

$$\begin{aligned} \delta\rho_{\alpha L}(r\omega) &= \sum_{\beta} \int dr' \tilde{R}_{0,qL}^{\alpha\beta}(rr'\omega) \left[ \sum_{\gamma} \kappa_{\beta\gamma}(r') \delta\rho_{\gamma L}(r'\omega)/r'^2 + \delta_{\beta,0q} f_{qL}(r') \right] \\ &+ 2 \sum_{\beta} S_q^{\alpha\beta}(r) \left[ \sum_{\gamma} \tilde{\kappa}_{\beta\gamma}(r) \delta\rho_{\gamma L}(r\omega)/r^2 + \delta_{\beta,0q} f_{qL}(r) \right] \end{aligned} \quad (21)$$

where

$$\delta\rho_{\alpha L} \in [\delta\rho_q]_L, [\delta\Delta + \rho_q]_L, [\delta\nabla\rho_q]_L^{\lambda=L\pm 1}, [\delta\tau_q]_L, [\delta 2i\mathbf{j}_q]_L^{\lambda=L\pm 1}, [\delta\tilde{\rho}_{\pm q}]_L. \quad (22)$$

Here  $\tilde{R}_{0,qL}^{\alpha\beta}$  denotes a part of the response function which contains only the regular parts of the derivatives of  $\mathcal{G}_{0,qlj}$ . Its expression is the same as that of  $R_{0,qL}^{\alpha\beta}$  (Eq.(18)) except that the derivatives of the Green's function, e.g.  $\overrightarrow{\partial} \mathcal{G}_{0,qlj}(rr', E) \overleftarrow{\partial}$  in Eq.(20) is replaced by the corresponding regular part  $\overrightarrow{\partial} \mathcal{G}_{0,qlj}(rr', E) \overleftarrow{\partial}$ . On the other hand, the second term of r.h.s. of Eq.(21) represents con-

tribution from the singular terms such as  $\frac{2m_q^*(r)}{\hbar^2} \delta(r-r')$ . The integral  $\int dr'$  disappears in this term because of the delta function. The expressions of  $S_q^{\alpha\beta}$  are given in Appendix. Note that  $S_q^{\alpha\beta}$  is a one-point function independent of the frequency  $\omega$ , expressed in terms of local quantities such as  $\rho_q(r)$ ,  $\tau_q(r)$ ,  $m_q^*(r)$  and their derivatives.

It is noted that the linear response equation (21) includes the fluctuation  $[\delta\tau_q]_L$  in the kinetic energy density

$\delta\rho_\alpha$	$\mathcal{A}^\alpha, \mathcal{B}^\alpha$	$\hat{O}^\alpha(\mathbf{r})$	$\hat{O}_{ijl'j'}^\alpha(r)$	$\kappa_{\alpha\beta}$
$\delta\rho_q$	$\begin{pmatrix} 2 & 0 \\ 0 & 0 \end{pmatrix}, \begin{pmatrix} 1 & 0 \\ 0 & -1 \end{pmatrix}$	1	1	$a_{qq'}$
$\delta\Delta_+\rho_q$		$\overleftarrow{\Delta} + \overrightarrow{\Delta}$	$\frac{\overleftarrow{\partial}^2}{\partial r^2} + \frac{\overrightarrow{\partial}^2}{\partial r^2} - \frac{l'(l'+1)}{r^2} - \frac{l(l+1)}{r^2}$	$b_{qq'}$
$\delta\nabla\rho_q$		$\overleftarrow{\nabla} + \overrightarrow{\nabla}$	$\begin{cases} \sqrt{\frac{L}{2L+1}} \left( \frac{\overleftarrow{\partial}}{\partial r} + \frac{\overrightarrow{\partial}}{\partial r} + \frac{L-1}{r} \right) & (\text{for } [\delta\nabla\rho_q]_L^{\lambda=L-1}) \\ -\sqrt{\frac{L+1}{2L+1}} \left( \frac{\overleftarrow{\partial}}{\partial r} + \frac{\overrightarrow{\partial}}{\partial r} - \frac{L+2}{r} \right) & (\text{for } [\delta\nabla\rho_q]_L^{\lambda=L+1}) \end{cases}$	$c_{qq'}$
$\delta\tau_q$		$\overleftarrow{\nabla} \cdot \overrightarrow{\nabla}$	$\frac{\overleftarrow{\partial}}{\partial r} \frac{\overrightarrow{\partial}}{\partial r} - \frac{1}{r} \frac{\overrightarrow{\partial}}{\partial r} - \frac{\overleftarrow{\partial}}{\partial r} \frac{1}{r} + \frac{l(l+1)+l'(l'+1)-(L+2)(L-1)}{2} \left( \frac{1}{r^2} \right)$	-
$\delta 2i\mathbf{j}_q$	$\begin{pmatrix} 2 & 0 \\ 0 & 0 \end{pmatrix}, \begin{pmatrix} 1 & 0 \\ 0 & 1 \end{pmatrix}$	$-\overleftarrow{\nabla} + \overrightarrow{\nabla}$	$\begin{cases} -\sqrt{\frac{L}{2L+1}} \left( \frac{\overleftarrow{\partial}}{\partial r} - \frac{\overrightarrow{\partial}}{\partial r} + \frac{l(l+1)-l'(l'+1)}{L} \frac{1}{r} \right) & (\text{for } [\delta 2i\mathbf{j}_q]_L^{\lambda=L-1}) \\ \sqrt{\frac{L+1}{2L+1}} \left( \frac{\overleftarrow{\partial}}{\partial r} - \frac{\overrightarrow{\partial}}{\partial r} - \frac{l(l+1)-l'(l'+1)}{L+1} \frac{1}{r} \right) & (\text{for } [\delta 2i\mathbf{j}_q]_L^{\lambda=L+1}) \end{cases}$	$-b_{qq'}$
$\delta\tilde{\rho}_{+q}$	$\begin{pmatrix} 0 & 1 \\ 1 & 0 \end{pmatrix}$	1	1	$\tilde{a}_q \delta_{qq'}$
$\delta\tilde{\rho}_{-q}$	$\begin{pmatrix} 0 & 1 \\ -1 & 0 \end{pmatrix}$	1	1	$-\tilde{a}_q \delta_{qq'}$

TABLE I: The correspondence and the expressions for the matrices  $\mathcal{A}^\alpha$  and  $\mathcal{B}^\beta$ , the operators  $\hat{O}^\alpha$  and  $\hat{O}_{ijl'j'}^\alpha$  and  $\kappa_{\alpha\beta}$  appearing in Eqs. (11), (14) and (18). See also the text and Appendix.

$\tau_q$  as a dynamical variable to be considered. This is because  $[\delta\tau_q]_L$  emerges from the singular terms associated with the linear response equation for  $[\delta\Delta_+\rho_q]_L$ . Finally we make a little remark on the structure of the singular terms. The presence of the singular terms has been notified in the formulation of the Skyrme-HF plus continuum RPA[40, 43] where the pairing is neglected. In the present Skyrme-HFB plus continuum QRPA approach, the structure of the singular terms is more involved since the response function contains two single-particle HFB

Green's functions (instead of one Green's function in the case of the continuum RPA[40, 43]). Looking at the expression of Eq.(18), it may appear that products of two delta functions  $\frac{2m_q^*(r)}{\hbar^2} \delta(r-r')$  emerge from the singular terms of two HFB Green's functions in Eq.(18). Such a term however does not contribute to the response function since it has no energy dependence and hence it vanishes when the contour integral in the complex energy plane is performed.

### III. NUMERICAL ANALYSIS

In this section, we shall demonstrate the Skyrme continuum QRPA by performing numerical calculations for the dipole and quadrupole responses in  $^{20}\text{O}$  and  $^{54}\text{Ca}$ .

#### A. Numerical procedure

Let us first describe the detailed procedure of the numerical calculation.

We adopt the SkM\* parameter set of the Skyrme interaction and the mixed-type parametrization of the DDDI pairing interaction ( $\eta = 0.5$ ,  $\gamma = 1$ ,  $\rho_0 = 0.16$

$\text{fm}^{-3}$ )[35] for most of the calculations. The force strength  $V_0$  of the DDDI is chosen so that the average neutron pairing gap  $\langle \Delta_n \rangle$  reproduces the overall magnitudes of the experimental odd-even mass differences for the isotopic chain, obtained with the three-point formula[45]. Here we use the average pairing gap defined by  $\langle \Delta_n \rangle = \int d\mathbf{r} \tilde{\rho}_n(\mathbf{r}) \Delta_n(\mathbf{r}) / \int d\mathbf{r} \tilde{\rho}_n(\mathbf{r})$ . The adopted value is  $V_0 = -280$  and  $-285 \text{ MeVfm}^{-3}$  for  $^{20}\text{O}$  and  $^{54}\text{Ca}$  producing  $\langle \Delta_n \rangle = 1.91 \text{ MeV}$  and  $1.29 \text{ MeV}$ , respectively.

Since we use the contact interaction for the effective pairing interaction, we need a cut-off of the quasi-particle states in the HFB calculation. We define the cut-off with respect to the quasi-particle energy  $E_\alpha < E_{max} = 60 \text{ MeV}$ . Concerning the angular momentum quantum numbers  $lj$  we sum up the quasi-particle states up to  $l_{max} = 7\hbar$  and  $8\hbar$  for  $^{20}\text{O}$  and  $^{54}\text{Ca}$ , respectively. In performing the HFB and the continuum QRPA calculations, we discretize the radial coordinate space up to  $r_{max} = 15 \text{ fm}$  with an equidistant interval  $\Delta r = 0.2 \text{ fm}$ . In the continuum QRPA calculations, the dynamical quantities to be obtained are the eighteen functions  $[\delta\rho_q]_L, [\delta\tilde{\rho}_{\pm q}]_L, [\delta\Delta + \rho_q]_L, [\delta\nabla\rho_q]_L^{\lambda=L\pm 1}, [\delta 2i\mathbf{j}_q]_L^{\lambda=L\pm 1}$  and  $[\delta\tau_q]_L$  which obey the linear response equation (21). Using the same radial mesh, these functions are represented as a grand vector while the linear response equation is represented as a linear algebraic equation where the response function  $\tilde{R}_{0,qL}^{\alpha\beta}$  (and  $S_q^{\alpha\beta}$ ) corresponds to a matrix. Since the number of the functions to be solved is larger (18 vs. 6) than in the previous continuum QRPA that handles only the local densities  $[\delta\rho_q]_L$  and  $[\delta\tilde{\rho}_{\pm q}]_L$ , the number of the matrix elements of the response functions is therefore about ten times larger than in the previous continuum QRPA calculations. To reduce the increased computational cost thus caused, we have chosen the values of  $l_{max}$  and  $r_{max}$  smaller than those used in our previous calculations [10, 11, 12, 13]. For the same reason we have used here a relatively large smearing parameter  $\epsilon = 1.0 \text{ MeV}$  in most of the following calculations. We evaluate the strength function at discretized excitation energies with an interval of  $0.5 \text{ MeV}$ .

It is noted here that the self-consistency is not completely satisfied in the present formulation since a few approximations are introduced in deriving the residual interaction from the Skyrme HFB functional. Consequently the spurious modes of motion which should have exact zero excitation energy according to the Thouless's theorem[6] do not emerge at the expected energy. A commonly adopted procedure to circumvent this problem is to renormalize the residual interaction  $\kappa_{\alpha\beta}$  in Eq.(21) by an overall factor  $f$  as  $\kappa_{\alpha\beta} \rightarrow f \times \kappa_{\alpha\beta}$  so that the excitation energy of the spurious mode is forced at the zero energy[10, 11, 12, 14, 15, 20, 21, 22, 46]. We apply this renormalization procedure to the particle-hole residual interactions that are derived from the Skyrme HF functional  $E_{\text{Skyrme}}$ . The residual interaction in the particle-particle channel, derived from the pair correlation energy  $E_{\text{pair}}$ , is kept in the original strength since

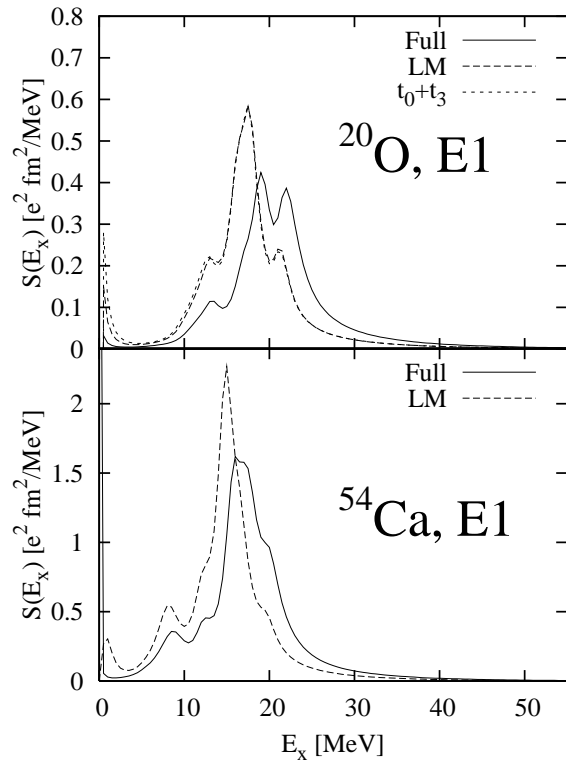


FIG. 1: The  $B(E1)$  strength function of isovector dipole response in  $^{20}\text{O}$  (upper panel) and in  $^{54}\text{Ca}$  (lower panel) calculated with the parameter set SkM\*. The solid curve is the result obtained in the full calculation while the dashed curve is that in the Landau-Migdal (LM) approximation. The dotted curve in the upper panel is the one in the  $t_0 + t_3$  approximation. See also the text.

the continuum QRPA in the Green's function formalism fulfills the self-consistency in the particle-particle channel with high accuracy [10, 11]. The renormalization factor is  $f = 1.0470$  and  $1.0142$  for  $^{20}\text{O}$  and  $^{54}\text{Ca}$ , respectively.

In the following analysis, we would like to demonstrate how the description of the multipole response is improved in comparison with the previous continuum QRPA where the residual interaction is simplified to a contact force. For this purpose, we perform calculations where the Landau-Migdal (LM) approximation to the residual interaction is introduced [13, 14, 15, 16, 17, 20, 21, 22]. This is an approximation which replaces the residual interaction by a contact force  $\propto \delta(\mathbf{r} - \mathbf{r}')$  whose strength is given by the density-dependent Landau-Migdal parameters  $F_0$  and  $F'_0$  evaluated for the Skyrme functional[9, 27, 28] using the local density approximation. It should be noted, however, that the Landau-Migdal parameters  $F_0$  and  $F'_0$  contain a part of the  $t_1$  and  $t_2$  terms, and this approximation should be distinguished from dropping all the  $t_1$  and  $t_2$  terms.

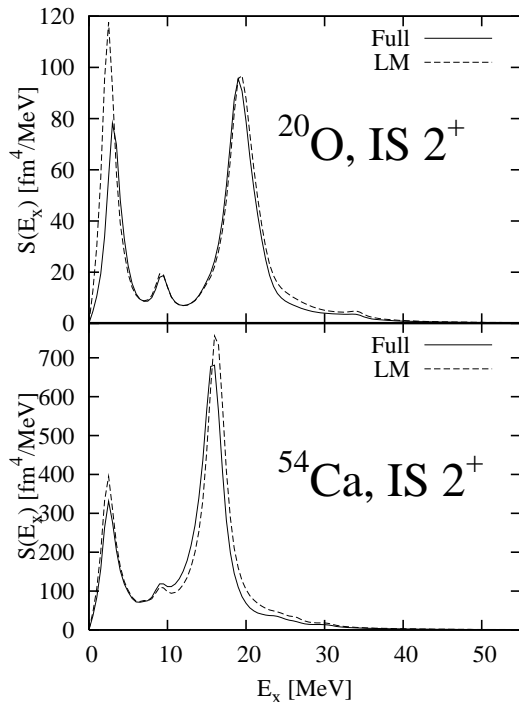


FIG. 2: The same as Fig.1 but for the  $B(\text{IS}2)$  isoscalar quadrupole strength function in  $^{20}\text{O}$  and  $^{54}\text{Ca}$ .

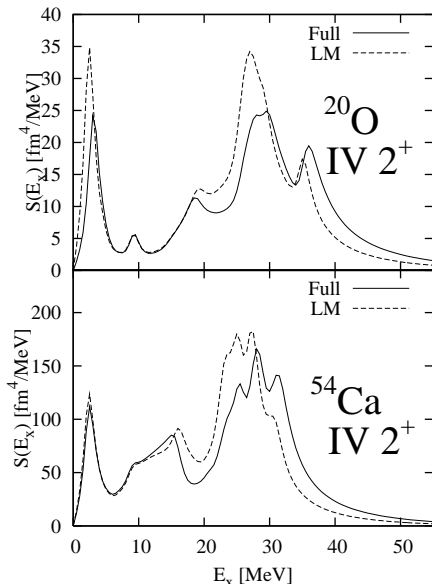


FIG. 3: The same as Fig.1 but for the  $B(\text{IV}2)$  isovector quadrupole strength function.

## B. Strength function

The strength function

$$S(\hbar\omega) \equiv \sum_{\nu, M} |\langle \nu | \hat{F}_{LM} | 0 \rangle|^2 \delta(\hbar\omega - E_\nu)$$

$$= -\frac{2L+1}{\pi} \text{Im} \sum_q \int dr f_{qL}(r) [\delta\rho_q]_L(r, \omega) \quad (23)$$

for the operator  $\hat{F}_{LM}$  with the multipolarity  $L$  can be evaluated in terms of the solution  $[\delta\rho_q]_L(r, \omega)$  of the linear response equation (21) obtained for the external field  $\hat{F}_{L0}$ . We evaluate the  $B(\text{E}1)$ ,  $B(\text{IS}2)$  and  $B(\text{IV}2)$  strength functions associated with the electric dipole operator

$$\hat{F}_{1M}^{IV} = \frac{eN}{A} \sum_{i=1}^Z r_i Y_{1M}(\Omega_i) - \frac{eZ}{A} \sum_{i=1}^N r_i Y_{1M}(\Omega_i) \quad (24)$$

and the isoscalar/isovector quadrupole operators

$$\hat{F}_{2M}^{IS} = \sum_{i=1}^A r_i^2 Y_{2M}(\Omega_i), \quad \hat{F}_{2M}^{IV} = \sum_{i=1}^A \tau_z r_i^2 Y_{2M}(\Omega_i). \quad (25)$$

The  $B(\text{E}1)$  strength functions calculated for  $^{20}\text{O}$  and  $^{54}\text{Ca}$  are shown with the solid curve in Fig.1. The broad peaks around  $E_x = 20$  MeV in  $^{20}\text{O}$  and  $E_x = 16$  MeV in  $^{54}\text{Ca}$  correspond to the giant dipole resonance (GDR). There is a small bump around  $E_x = 8$  MeV in  $^{54}\text{Ca}$ , which corresponds to the soft dipole excitation or the pygmy dipole resonance. We find however that the small peak  $E_x = 13$  MeV in  $^{20}\text{O}$  is neither the GDR nor the soft dipole excitation, but rather a non-collective two-quasiparticle excitation (cf. Section III D). The strength at  $E \approx 0$  is due to the spurious mode, and it is caused by the incomplete self-consistency.

For the sake of comparison, the  $B(\text{E}1)$  strength function obtained in the Landau-Migdal (LM) approximation of the residual interaction is also plotted with the dashed curve in Fig.1. Note that the renormalization factor used in the Landau-Migdal approximation ( $f = 0.6686$  and  $0.7515$  for  $^{20}\text{O}$  and  $^{54}\text{Ca}$ , respectively) deviate significantly from one in contrast to those in the full calculation ( $f = 1.0470$  and  $1.0142$ ). This fact suggests that there is significant improvement in the self-consistency compared with the LM approximation. This feature is pointed out in a Skyrme-QRPA calculation using discretized continuum quasiparticle states[21].

It is seen in Fig.1 that the profile of the strength function obtained in the LM approximation differs significantly from that in the full calculation. The peak positions of the giant dipole resonance are apparently different. Estimating the centroid energy of the GDR by  $E(\text{GDR}) = m_1/m_0$  using the energy weighted sum  $m_1$  and the non-weighted sum  $m_0$ , we find  $E(\text{GDR}) = 20.66$  MeV ( $^{20}\text{O}$ ) and  $15.80$  MeV ( $^{54}\text{Ca}$ ) for the full calculation while  $E(\text{GDR}) = 17.67$  and  $14.20$  MeV in the LM approximation, exhibiting a rather large difference by about 2-3 MeV. It is clear that the LM approximation is not very appropriate to give precise quantitative description of the GDR.

If we evaluate the energy weighted sum integrated up to  $E = 15$  MeV for  $^{20}\text{O}$ , the full calculation gives 9.7 % of

the classical Thomas-Reiche-Kuhn (TRK) sum rule value while it is 20.1% in the LM approximation. Comparing with the experimental value 12%[47], we find that the full calculation is in better agreement with the experiment. The  $B(E1)$  strength function in  $^{20}\text{O}$  is calculated in a fully self-consistent Skyrme-QRPA calculation[24] using the same SkM\*. We find only small difference between our calculation and that in Ref.[24]. It may be attributed to the neglect of the Coulomb and spin-dependent terms in our calculations. The observed effect of the velocity dependent terms on the GDR centroid energy is essentially the same as that discussed in Ref.[21].

Figure 2 displays the  $B(\text{IS}2)$  isoscalar strength function for the quadrupole responses in  $^{20}\text{O}$  and  $^{54}\text{Ca}$ . In both nuclei there are two significant peaks, one around  $E_x = 2 - 3$  MeV corresponding to the low-lying  $2^+$  collective vibrational mode and the other around  $E_x = 15 - 20$  MeV corresponding to the isoscalar giant quadrupole resonance (ISGQR). (The experimental  $2_1^+$  energy in  $^{20}\text{O}$  is 1670 keV[48].) The calculated isoscalar quadrupole strength function for  $^{54}\text{Ca}$  is quite similar to that obtained in the fully self-consistent Skyrme QRPA using the same SkM\*[24] apart from features associated with different choices of the smoothing width.

Concerning the effect of the velocity dependent terms, it is seen in Fig. 2 that the difference between the full calculation and the LM approximation is less significant in comparison with the isovector dipole response: the peak positions of the giant isoscalar quadrupole resonance ( $E = 19.0$  MeV) and of the low-lying state ( $E = 3.0$  MeV) in  $^{20}\text{O}$  is affected only little by inclusion of the velocity dependent terms. The same is seen also in  $^{54}\text{Ca}$ . Note however that the influence of the velocity dependent terms on the  $B(\text{IV}2)$  isovector distribution is clearly larger than in the case of the  $B(\text{IS}2)$  isoscalar strength distribution as is seen in Fig.3. Combining Figs. 1, 2 and 3, we see an apparent trend that the influence of the velocity-dependent terms is more significant in the isovector responses than in the isoscalar responses.

Before moving to the next subsection, we would like to make a few additional remarks on the effect of the velocity dependent terms. We first remark that it is possible to consider another way to evaluate the effect of the velocity dependent terms, e.g. by comparing with a calculation where all the velocity dependent terms containing the  $t_1$  and  $t_2$  parameters are completely neglected. (In other words, it is the calculation where only the simple contact interaction associated with the  $t_0$  and  $t_3$  terms are taken into account. It is different from the Landau-Migdal (LM) approximation since in the latter a part of the  $t_1$  and  $t_2$  terms is renormalized into the Landau-Migdal parameters  $F_0$  and  $F'_0$ .) The  $B(E1)$  strength function in this  $t_0 + t_3$  approximation calculated for  $^{20}\text{O}$  is plotted in the upper panel of Fig.1 together with the other two curves representing the full calculation and the LM approximation. We find here that the result obtained in the  $t_0 + t_3$  approximation is almost identical to that in the LM approximation. Secondly, we remark that the effect

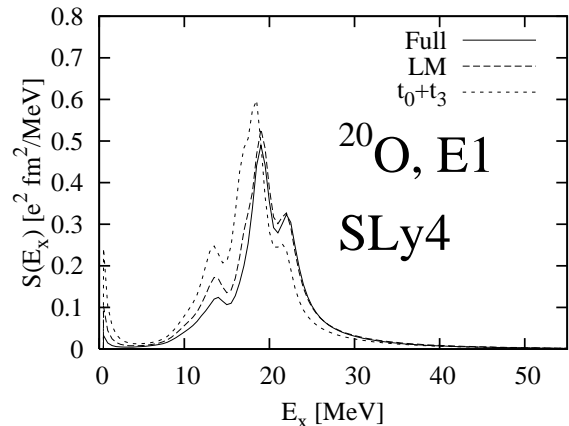


FIG. 4: The same as the upper panel of Fig.1, but the Skyrme parameter set SLy4 is used.

of the velocity dependent terms depends on the adopted Skyrme parameter set. To demonstrate this we show in Fig.4 the  $B(E1)$  strength function in  $^{20}\text{O}$  obtained with SLy4[33] instead of SkM\*. It is seen that there is no big difference in the GDR peak position between the full calculation and in the Landau-Migdal approximation, and hence the effect of the velocity dependent terms in the case of SLy4 appears smaller than in the case of SkM\*. Note however that even in this case there is significant difference between the LM and  $t_0 + t_3$  approximations. If we look at the difference between the full calculation and the  $t_0 + t_3$  approximation, the effect of the velocity dependent terms is not negligible. Note also that the difference between the full calculation and the LM approximation is not negligible in the sum rule (cf. next subsection).

### C. Energy weighted sum rule

Let us analyze whether the energy weighted sum rule is satisfied in the present calculations. For this purpose we evaluate the running energy weighted sum defined by

$$W(E_x) = \int_0^{E_x} dE E S(E), \quad (26)$$

which integrates the sum up to an excitation energy  $E_x$ . The limiting value of  $W(E_x)$  for a sufficiently large  $E_x$  is to be compared with the energy-weighted sum rule (EWSR).

The EWSR for the  $B(\text{IS}L)$  isoscalar multipole strength function is identical to the classical sum rule  $m_1^{cl} \equiv \frac{1}{4\pi} \frac{\hbar^2}{2m} L(2L+1)^2 A \langle r^{2L-2} \rangle$  which is expressed in terms of the expectation value of the radial moment  $r^{2L-2}$  with respect to the ground state[6, 38]. For the isovector multipole strength functions, however, the EWSR contains the enhancement factor which arises from the residual interaction, in particular the velocity-dependent terms in the case of the Skyrme effective force[36, 38, 39, 49, 50].

The EWSR for the  $B(E1)$  electric dipole strength function is given by  $m_1^{\text{EWSR}}(E1) = \frac{NZ}{A^2} m_1^{\text{cl}} (1 + \kappa)$  where  $\kappa$  is the enhancement factor which is easily evaluated in the case of the Skyrme force[23, 51]. The value of  $\kappa$  for SkM\* is  $\kappa = 0.32$  and  $0.36$  in  $^{20}\text{O}$  and  $^{54}\text{Ca}$ , respectively.

The upper panel of the Fig.5 displays the running energy weighted sum  $W(E_x)$  for the  $B(E1)$  strength function of the dipole response in  $^{20}\text{O}$  (cf. Fig.1). The running sum evaluated at the highest calculated energy  $E_x = 55$  MeV reaches 96% of the EWSR. This suggests that the EWSR is satisfied in the present calculation. It is noted that  $W(E_x)$  approaches the EWSR value including the enhancement factor, but not the classical TRK value plotted with the dotted horizontal line in Fig. 5. Namely the effect of the velocity dependent terms in the residual interaction is indeed included in the present calculation. In the same figure, we also show the result obtained in the LM approximation. In this case, however, the running sum reaches only 86 % of the EWSR, and hence the approximation fails to describe the EWSR and the enhancement factor. The fluctuations  $\delta\Delta_{+\rho}$ ,  $\delta\nabla\rho$ ,  $\delta\tau$  and, in particular,  $\delta 2ij$  play the essential role to restore the EWSR since these are the fluctuations associated with the velocity-dependent terms ( $\propto t_1$  and  $t_2$ ). Note that the LM approximation neglects these fluctuations although a part of the velocity-dependent  $t_1 + t_2$  terms is taken into account via the Landau-Migdal parameters  $F_0$  and  $F'_0$ .

The lower panel in Fig.5 displays the running energy weighted sum for the  $B(\text{IS}2)$  isoscalar quadrupole strength function in  $^{54}\text{Ca}$  (cf. Fig.2). The energy weighted sum amounts to 98% of the EWSR, and we confirm more clearly than in the analysis of the electric dipole strength that the EWSR is satisfied in the present calculation. When we adopt the LM approximation where the fluctuations  $\delta\Delta_{+\rho}$ ,  $\delta\nabla\rho$ ,  $\delta\tau$  and  $\delta 2ij$  are neglected, the running sum  $W(E_x)$  at the maximum energy  $E_x = 55$  MeV overshoots the EWSR by about ten percent. Again the consistent inclusion of the velocity dependent terms in the QRPA description is essential to guarantee the EWSR. It is noted also that the difference between the full calculation and the Landau-Migdal approximation is significant mainly in the energy region ( $E_x > 18$  MeV) higher than the giant resonance peak.

We confirmed that the EWSR is satisfied also in the case of the other Skyrme parameter set SLy4. For the  $B(E1)$  and  $B(\text{IS}2)$  strength functions in  $^{20}\text{O}$ , the running sum  $W(E_x)$  at the highest energy  $E_x = 55$  MeV reaches 95% and 97% of the EWSR, respectively. In the LM approximation, on the contrary, the sum overshoots the EWSR by 6% and 12% in the  $B(E1)$  and  $B(\text{IS}2)$  strength functions, respectively.

In Fig.6, we demonstrate influence of the residual pairing interaction on the energy-weighted sum. When the residual pairing interaction is dropped in the continuum QRPA calculation (i.e., the dynamical pairing effect is neglected), the energy-weighted sum overestimates the EWSR value by 5%. As pointed out already[10, 11, 18],

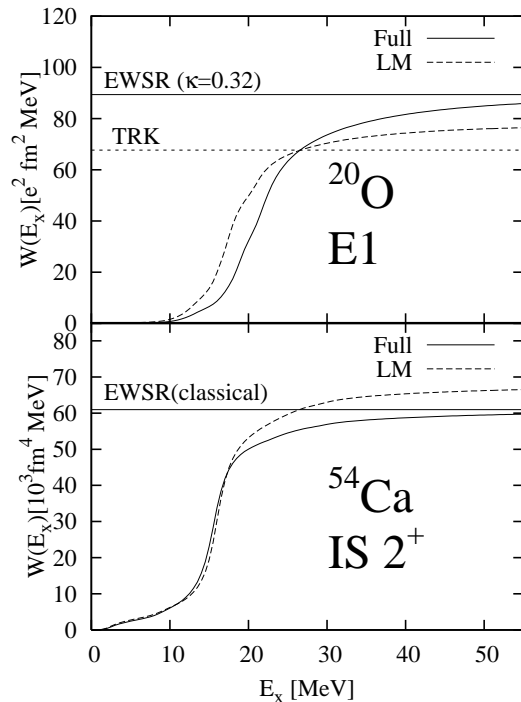


FIG. 5: The running energy weighted sum for the  $B(E1)$  electric dipole strength function in  $^{20}\text{O}$ (upper panel) and that for the  $B(\text{IS}2)$  isoscalar quadrupole strength function in  $^{54}\text{Ca}$ (lower panel) obtained using the Skyrme parameter set SkM\*. The solid curve represents the result of the full calculation of the present Skyrme continuum QRPA while the dashed curve is the result obtained in the Landau-Migdal (LM) approximation to the residual interaction. The horizontal solid line indicates the value of the energy-weighted sum rule in the present calculation, which includes the enhancement factor in the isovector response. The dotted horizontal line in the upper panel denotes the value of the Thomas-Reiche-Kuhn sum rule.

inclusion of the dynamical pairing effect is important to guarantee the energy weighted sum-rule because otherwise the self-consistency in the pairing channel would be violated. This means, in the present context, that we need to include both the velocity dependent terms of the Skyrme effective interaction and the residual pairing interaction.

Figures 7 and 8 show the  $B(E1)$  and  $B(\text{IS}2)$  strength functions in  $^{20}\text{O}$ , respectively, calculated with use of a small smearing width  $\epsilon = 0.2$  MeV. They are compared with those obtained with  $\epsilon = 1.0$  MeV (cf. Figs.1 and 2). The running energy weighted sum of the strength functions is also shown. Finer structures of the strength functions are visible here: we can distinguish the first excited  $2^+$ , which is a bound discrete state located below the separation energy.

It is seen from the bottom panels of Figs. 7 and 8 that the agreement with the energy weighted sum rule is improved with use of the smaller smearing width. The running sums at the highest energy  $E_x = 55(50)$  MeV

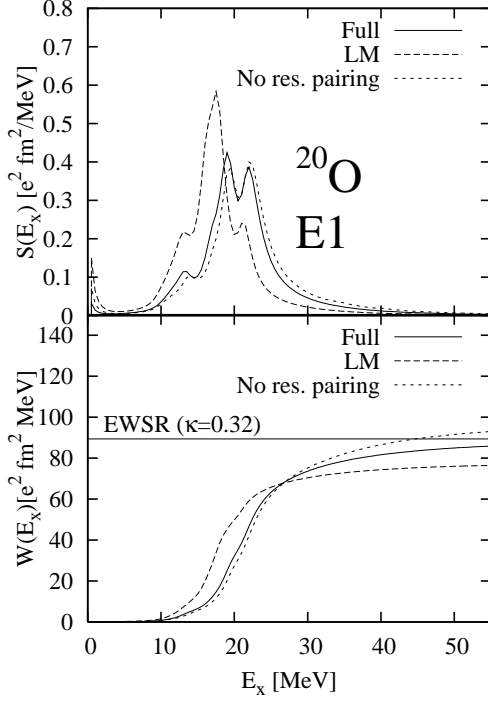


FIG. 6: The  $B(E1)$  strength function (upper panel) and its running energy-weighted sum (lower panel) for the isovector dipole response of  $^{20}\text{O}$  using SkM\*. The solid and dashed curves are the results obtained in the full calculation and in the Landau-Migdal approximation, respectively, while the dotted curve is the one in which we neglect the residual pairing interaction in the continuum QRPA.

are 98 and 98 % for the  $B(E1)$  and  $B(\text{IS}2)$  strengths, respectively, which should be compared with the corresponding values 96 % and 96 % obtained with  $\epsilon = 1.0$  MeV.

In the following we return to  $\epsilon = 1.0$  MeV since calculations with  $\epsilon = 0.2$  MeV demand very long computation time.

#### D. Transition densities

Let us now look into individual modes of excitation. For this purpose we analyze the transition densities associated with each excitation mode. We evaluate three kinds of transition densities [12, 14, 15, 52]

$$\rho_{iq}^{ph}(\mathbf{r}) = \langle \Phi_i | \sum_{\sigma} \psi_q^{\dagger}(\mathbf{r}\sigma) \psi_q(\mathbf{r}\sigma) | \Phi_0 \rangle = Y_{LM}^*(\hat{\mathbf{r}}) \rho_{iqL}^{ph}(r), \quad (27)$$

$$P_{iq}^{pp}(\mathbf{r}) = \langle \Phi_i | \psi_q^{\dagger}(\mathbf{r}\uparrow) \psi_q^{\dagger}(\mathbf{r}\downarrow) | \Phi_0 \rangle = Y_{LM}^*(\hat{\mathbf{r}}) P_{iqL}^{pp}(r), \quad (28)$$

$$P_{iq}^{hh}(\mathbf{r}) = \langle \Phi_i | \psi_q(\mathbf{r}\downarrow) \psi_q(\mathbf{r}\uparrow) | \Phi_0 \rangle = Y_{LM}^*(\hat{\mathbf{r}}) P_{iqL}^{hh}(r) \quad (29)$$

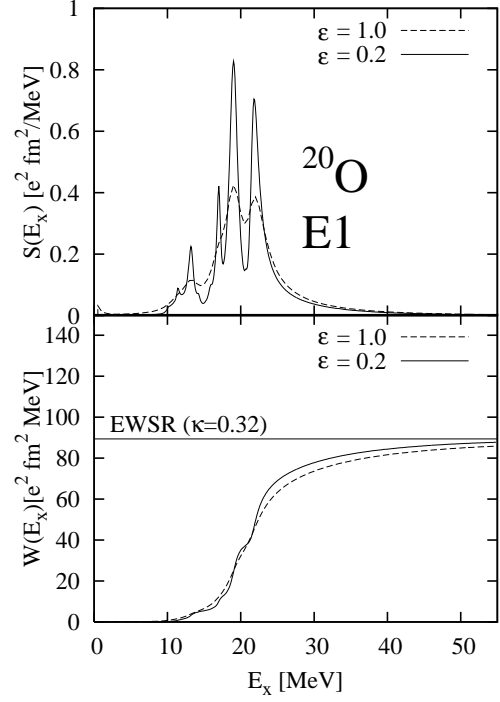


FIG. 7: The  $B(E1)$  strength function in  $^{20}\text{O}$  (upper panel) and its running energy weighted sum (lower panel) which are obtained with a small smoothing width parameter  $\epsilon=0.2$  MeV. For comparison, the results obtained with  $\epsilon=1.0$  MeV, shown already in Fig.6, are also plotted with the dashed curves.

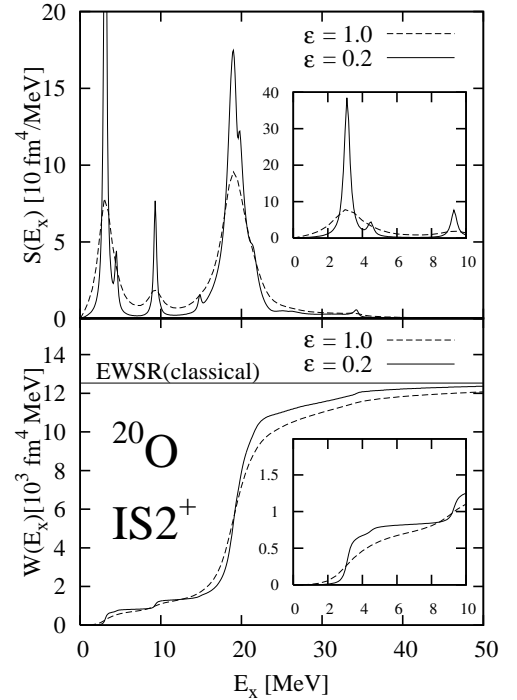


FIG. 8: The same as Fig.7, but for the  $B(\text{IS}2)$  strength function in  $^{20}\text{O}$ .

using the solution of the linear response equation (21) at an energy corresponding to a peak in the strength function. Here  $\rho_{iq}^{ph}(\mathbf{r})$  is the usual particle-hole transition density while  $P_{iq}^{pp}(\mathbf{r})$  and  $P_{iq}^{hh}(\mathbf{r})$  are the particle-pair and hole-pair transition densities associated with the pair addition and removal amplitudes, respectively.

Let us first discuss the giant dipole resonance (GDR) and the low-lying small peak seen in the  $B(E1)$  strength function. We focus on  $^{54}\text{Ca}$ , where we find two peaks at  $E_x = 8.5$  MeV and 16.0 MeV in the strength function shown in Fig.1. (The corresponding peaks in the Landau-Migdal approximation are found at  $E_x = 8.0$  and 15.0 MeV.) The transition densities evaluated at  $E_x = 16.0$  MeV is shown in Fig.9(a). It is seen that the particle-hole transition density  $\rho_{iqL}^{ph}(r)$  is large around the nuclear surface, and that the neutron and proton amplitudes have the opposite phases. This is indeed the feature typical of the isovector giant dipole resonance (GDR). The character of the excitation mode at  $E_x = 8.5$  MeV is different from that of the giant resonance. This is seen in the transition densities shown in Fig.9(b), where we find a characteristic feature that the neutron amplitude of the particle-hole transition density dominates over the proton's in the exterior of the nucleus. The neutron amplitude has a node around the nuclear surface, and it exhibits significant magnitude also inside the surface, where the proton amplitude also has comparable magnitude with the same phase as that of the neutron. This is the feature which is often interpreted as the soft dipole excitation or the pygmy dipole resonance characteristic to neutron-rich nuclei[12, 18, 42, 53, 54].

It is interesting to check how well the Landau-Migdal approximation can describe the transition densities and the mode characters. This is a non-trivial question since we have already seen that there is rather large difference in the  $B(E1)$  strength functions between in the full calculation and the Landau-Migdal approximation. The transition densities evaluated at  $E_x = 15.0$  and 8.0 MeV are shown in the panels (c) and (d) in Fig.9, which are compared with those in (a) and (b). In both the cases of the giant dipole resonance ((a) vs. (c)) and of the soft dipole excitation ((b) vs. (d)), the basic features of the transition densities are the same in the full and LM calculations, although we see small but non-negligible differences, e.g., in the relative size between the particle-hole transition density  $\rho^{ph}(r)$  and the particle-pair transition density  $P^{pp}(r)$  for the neutrons. This comparison suggests that the Landau-Migdal approximation can be used to describe the basic structure of these excitation modes while some reservation should be held when aiming at a quantitative description.

Similar analysis of the transition densities is performed also for the isoscalar quadrupole modes in  $^{54}\text{Ca}$ . We analyze here the isoscalar giant quadrupole resonance having a broad peak around  $E_x = 16.0$  MeV and the low-lying quadrupole vibrational state peaked around  $E_x = 2.5$  MeV. The transition densities evaluated at these peak energies are plotted in Fig.10 (a) and (b). The transi-

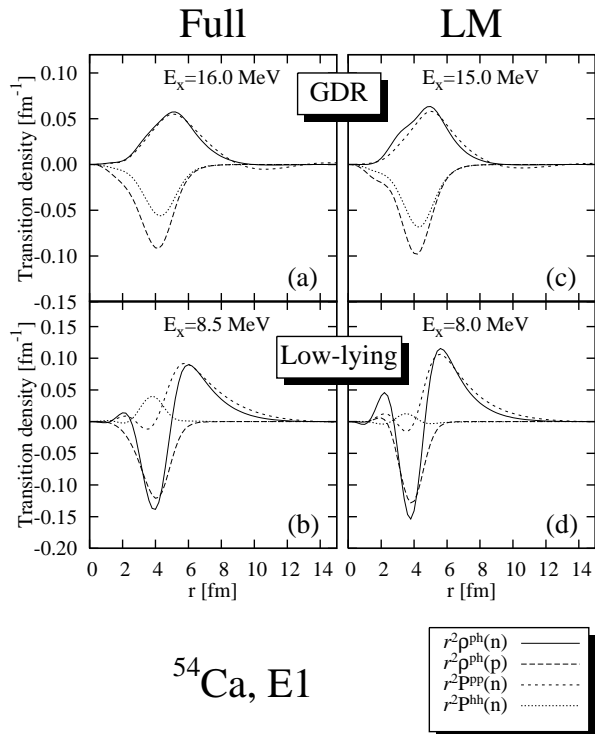


FIG. 9: The transition densities  $r^2 \rho_{iqL}^{ph}(r)$ ,  $r^2 P_{iqL}^{pp}(r)$  and  $r^2 P_{iqL}^{hh}(r)$  for the isovector dipole response in  $^{54}\text{Ca}$ . (a) and (b) are those in the full calculation, evaluated at  $E_x = 16.0$  MeV (the peak energy of the GDR) and  $E_x = 8.5$  MeV (the peak energy of the soft dipole excitation), respectively. (c) and (d) are those in the Landau-Migdal approximation. We here plot the neutron amplitudes weighted with the volume element  $r^2$  for the three kinds of transition densities. For the proton we plot only  $r^2 \rho_{iqL}^{ph}(r)$ . Note that we need to normalize the transition densities in terms of the  $B(E1)$  strength of this mode[12], but we assume here the unit strength  $B(E1)=1 \text{ e}^2 \text{ fm}^2$ .

tion densities of the corresponding peaks in the Landau-Migdal approximation are also plotted in (c) and (d). Comparing the full calculation and the Landau-Migdal approximation, we observe the same trends as found in the case of the giant dipole resonance and the soft dipole excitation. Namely there is no difference in the basic features of the modes, but quantitative details of the transition densities depend on whether the velocity-dependent terms of the Skyrme interaction are taken account or not.

We analyzed also the transition densities evaluated at the peaks of the dipole and quadrupole strength functions in  $^{20}\text{O}$ . We obtained results similar to those in  $^{54}\text{Ca}$  except for the low-lying peak at  $E_x = 8.5$  MeV in the dipole response. The transition densities corresponding to this peak is different from those of the GDR nor those of the soft dipole excitation. We infer this peak as having non-collective nature.

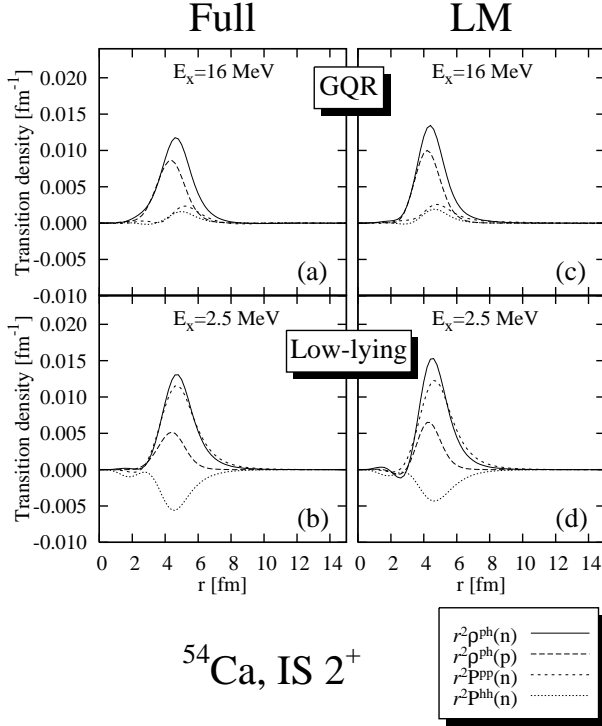


FIG. 10: The same as Fig.9 but for the isoscalar quadrupole response in  $^{54}\text{Ca}$ . (a) and (b) are those in the full calculation, evaluated at  $E_x = 16.0$  MeV (the peak energy of the ISGQR) and  $E_x = 2.5$  MeV (the peak energy of the low-lying surface vibration), respectively. (c) and (d) are those in the Landau-Migdal approximation. Note that we here normalized the transition densities in terms of the unit strength  $B(\text{IS}2)=1 \text{ fm}^4$ .

#### IV. CONCLUSIONS

We have developed the continuum QRPA which is based on the Skyrme-Hartree-Fock-Bogoliubov energy functional. In deriving the residual interaction used in the QRPA, we have taken into account the velocity-dependent central terms (proportional to the  $t_1$  and  $t_2$  coefficients) of the Skyrme effective interaction in order to guarantee the energy weighted sum rule for the multipole responses, but we neglected the two-body spin-orbit, the spin-spin and the Coulomb interactions.

The new continuum QRPA is applied to the isovector dipole and the isoscalar/isovector quadrupole responses of medium-mass neutron rich nuclides  $^{20}\text{O}$  and  $^{54}\text{Ca}$  using the SkM\* parameter set. It is confirmed numerically that the energy weighted sum rule is satisfied up to the enhancement factor relevant for the isovector responses. This is because the velocity dependent terms are taken into account in a way consistent with the Hartree-Fock-Bogoliubov mean-fields of the ground state. We thus constructed the first Skyrme continuum QRPA formalism that satisfies the sum rule.

We have also examined the importance of the velocity

dependent terms by comparing with the reduced calculation where the Landau-Migdal approximation is introduced to the residual interaction. The continuum QRPA using the Landau-Migdal approximation gives an overall correct description of the multipole responses, but influences of the approximation are seen in the shift of the centroid energy by 2-3 MeV of the isovector giant resonances and also in the violation of the energy weighted sum rule by about 10-15 % in the case of SkM\*. We found also small but non-negligible influence in the transition densities for the low-lying dipole and quadrupole modes. Note however that the qualitative features of the transition densities are described well even in this case, and only very little influence is seen in the case of the giant resonances. The analysis gives a partial justification for the use of the Landau-Migdal approximation.

#### Acknowledgments

The authors thank T. Inakura for valuable discussions and giving us data of the strength function in RPA for debugging our numerical code. The numerical calculations were performed on the NEC SX-8 supercomputer systems at Yukawa Institute for Theoretical Physics, Kyoto University, and at Research Center for Nuclear Physics, Osaka University. The work was supported by the Grant-in-Aid for Scientific Research(No.17540244) from the Japan Society for the Promotion of Science, and also by the JSPS Core-to-Core Program, International Research Network for Exotic Femto Systems(EFES).

#### DETAILS OF THE LINEAR RESPONSE EQUATION

Here we give some details of the linear response equation (21). The functions  $a_{qq'}$ ,  $b_{qq'}$ ,  $c_{qq'}$  and  $\tilde{a}_q$  appearing in Table I and Eqs.(9) and (10) are expressed as follows in terms of the effective interaction parameters and the local densities:

$$a_{qq'} = \begin{cases} \left. \begin{aligned} & \frac{1}{2}t_0(1-x_0) \\ & +(\alpha+2)(\alpha+1)\frac{1}{12}t_3(1+\frac{1}{2}x_3)\rho^\alpha \\ & -\frac{1}{12}t_3(x_3+\frac{1}{2}) \\ & \times \left[ \alpha(\alpha-1)\rho^{\alpha-2} \sum_{q''} \rho_{q''}^2 \right. \\ & \qquad \qquad \qquad \left. +4\alpha\rho^{\alpha-1}\rho_q + 2\rho^\alpha \right] \end{aligned} \right\} (q=q') \\ \left. \begin{aligned} & t_0(1+\frac{1}{2}x_0) \\ & +(\alpha+2)(\alpha+1)\frac{1}{12}t_3(1+\frac{1}{2}x_3)\rho^\alpha \\ & -\frac{1}{12}t_3(x_3+\frac{1}{2}) \\ & \times \left( \alpha(\alpha-1)\rho^{\alpha-2} \sum_{q''} \rho_{q''}^2 + 2\alpha\rho^\alpha \right) \end{aligned} \right\} (q \neq q') \end{cases}$$

$$b_{qq'} = \begin{cases} \left. \begin{aligned} & -\frac{1}{16}(t_1(1-x_1) + 3t_2(1+x_2)) \end{aligned} \right\} (q=q') \\ \left. \begin{aligned} & -\frac{1}{8}\{t_1(1+\frac{1}{2}x_1) + t_2(1+\frac{1}{2}x_2)\} \end{aligned} \right\} (q \neq q') \end{cases}$$

$\delta\rho_\alpha$	$2 \sum_{\beta\gamma} S_q^{\alpha\beta} [\tilde{\kappa}_{\beta\gamma} \delta\rho_{\gamma L}/r^2 + \delta_{\beta 0} f_{qL}]$
$[\delta\rho_q]_L$	$2 \times \frac{2m_q^*}{\hbar^2} \rho_q \sum_{q'} b_{qq'} [\delta\rho_{q'}]_L$
$[\delta\tilde{\rho}_{+q}]_L$	$2 \times \frac{2m_q^*}{\hbar^2} \tilde{\rho}_q \sum_{q'} b_{qq'} [\delta\rho_{q'}]_L$
$[\delta\tilde{\rho}_{-q}]_L$	0
$[\delta\Delta + \rho_q]_L$	$2 \times \frac{2m_q^*}{\hbar^2} \left\{ \rho_q \sum_{q'} a_{qq'} [\delta\rho_{q'}]_L + \tilde{\rho}_q \tilde{a}_q [\delta\tilde{\rho}_{+,q}]_L + 2(\Delta\rho_q - 2\tau_q) \sum_{q'} b_{qq'} [\delta\rho_{q'}]_L \right.$ $+ \rho_q \sum_{q'} (b_{qq'} - c_{qq'}) ([\delta\Delta + \rho_{q'}]_L + 2[\delta\tau_{q'}]_L) + \frac{\partial\rho_q}{\partial r} \sum_{q'} b_{qq'} \left( \sqrt{\frac{L}{2L+1}} [\delta\nabla\rho_{q'}]_L^{\lambda=L-1} - \sqrt{\frac{L+1}{2L+1}} [\delta\nabla\rho_{q'}]_L^{\lambda=L+1} \right)$ $\left. - \frac{2m_q^*}{\hbar^2} \left( \frac{\partial}{\partial r} \frac{\hbar^2}{2m_q^*} \right) \rho_q \sum_{q'} (b_{qq'} - c_{qq'}) \left( \sqrt{\frac{L}{2L+1}} [\delta\nabla\rho_{q'}]_L^{\lambda=L-1} - \sqrt{\frac{L+1}{2L+1}} [\delta\nabla\rho_{q'}]_L^{\lambda=L+1} \right) \right\} + 2 \times \frac{2m_q^* r^2}{\hbar^2} f_{qL}(r)$
$[\delta\nabla\rho_q]_L^{\lambda=L-1}$	$2 \times \frac{2m_q^*}{\hbar^2} \left\{ \sqrt{\frac{L}{2L+1}} \frac{\partial\rho_q}{\partial r} \sum_{q'} b_{qq'} [\delta\rho_{q'}]_L + \rho_q \sum_{q'} (b_{qq'} - \frac{L}{2L+1} c_{qq'}) [\delta\nabla\rho_{q'}]_L^{\lambda=L-1} + \frac{\sqrt{L(L+1)}}{2L+1} \rho_q \sum_{q'} c_{qq'} [\delta\nabla\rho_{q'}]_L^{\lambda=L+1} \right\}$
$[\delta\nabla\rho_q]_L^{\lambda=L+1}$	$2 \times \frac{2m_q^*}{\hbar^2} \left\{ -\sqrt{\frac{L+1}{2L+1}} \frac{\partial\rho_q}{\partial r} \sum_{q'} b_{qq'} [\delta\rho_{q'}]_L + \frac{\sqrt{L(L+1)}}{2L+1} \rho_q \sum_{q'} c_{qq'} [\delta\nabla\rho_{q'}]_L^{\lambda=L-1} + \rho_q \sum_{q'} (b_{qq'} - \frac{L+1}{2L+1} c_{qq'}) [\delta\nabla\rho_{q'}]_L^{\lambda=L+1} \right\}$
$[\delta 2i\mathbf{j}_q]_L^{\lambda=L-1}$	$-2 \times \frac{2m_q^*}{\hbar^2} \left\{ \frac{L}{2L+1} \rho_q \sum_{q'} b_{qq'} [\delta 2i\mathbf{j}_{q'}]_L^{\lambda=L-1} - \frac{\sqrt{L(L+1)}}{2L+1} \rho_q \sum_{q'} b_{qq'} [\delta 2i\mathbf{j}_{q'}]_L^{\lambda=L+1} \right\}$
$[\delta 2i\mathbf{j}_q]_L^{\lambda=L+1}$	$2 \times \frac{2m_q^*}{\hbar^2} \left\{ \frac{\sqrt{L(L+1)}}{2L+1} \rho_q \sum_{q'} b_{qq'} [\delta 2i\mathbf{j}_{q'}]_L^{\lambda=L-1} - \frac{L+1}{2L+1} \rho_q \sum_{q'} b_{qq'} [\delta 2i\mathbf{j}_{q'}]_L^{\lambda=L+1} \right\}$
$[\delta\tau_q]_L$	$2 \times \frac{2m_q^*}{\hbar^2} \left\{ \tau_q \sum_{q'} b_{qq'} [\delta\rho_{q'}]_L + \frac{1}{2} \frac{\partial\rho_q}{\partial r} \sum_{q'} (b_{qq'} - c_{qq'}) \left( \sqrt{\frac{L}{2L+1}} [\delta\nabla\rho_{q'}]_L^{\lambda=L-1} - \sqrt{\frac{L+1}{2L+1}} [\delta\nabla\rho_{q'}]_L^{\lambda=L+1} \right) \right\}$

TABLE II: The second term of r.h.s. of the linear response equation(21)

$$c_{qq'} = \begin{cases} -\frac{1}{16} (t_1(x_1 - 1) + 9t_2(x_2 + 1)) & (q = q') \\ \frac{1}{8} \{t_1(1 + \frac{1}{2}x_1) - 3t_2(1 + \frac{1}{2}x_2)\} & (q \neq q') \end{cases} \quad \tilde{a}_q = \frac{V_0}{2} \left[ 1 - \eta \left( \frac{\rho(r)}{\rho_0} \right)^\gamma \right].$$

- [1] I. Tanihata, H. Hamagaki, O. Hashimoto, Y. Shida, N. Yoshikawa, K. Sugimoto, O. Yamakawa, T. Kobayashi, and N. Takahashi, Phys. Rev. Lett. **55**, 2676 (1985).
- [2] A. Ozawa, O. Bochkarev, L. Chulkov, D. Cortina, H. Geissel, M. Hellström, M. Ivanov, R. Janik, K. Kimura, T. Kobayashi, *et al.*, Nucl. Phys. **A691**, 599 (2001).
- [3] T. Aumann, Euro. Phys. J. A **26**, 441 (2005).
- [4] J. Dobaczewski, H. Flocard, and J. Treiner, Nucl. Phys. **A422**, 103 (1984).
- [5] J. Dobaczewski, W. Nazarewicz, T. R. Werner, J. F. Berger, C. R. Chinn, and J. Decharge, Phys. Rev. C **53**, 2809 (1996).
- [6] P. Ring and P. Schuck, *The Nuclear Many-Body Problem* (Springer-Verlag, Berlin, 1980).
- [7] A. Bulgac, nucl-th/9907088.
- [8] J. Engel, M. Bender, J. Dobaczewski, W. Nazarewicz, and R. Surman, Phys. Rev. C **60**, 014302 (1999).
- [9] M. Bender, J. Dobaczewski, J. Engel, and W. Nazarewicz, Phys. Rev. C **65**, 054322 (2002).
- [10] M. Matsuo, Nucl. Phys. **A696**, 371 (2001).
- [11] M. Matsuo, Prog. Theor. Phys. Suppl. **146**, 110 (2002).
- [12] M. Matsuo, K. Mizuyama, and Y. Serizawa, Phys. Rev. C **71**, 064326 (2005).
- [13] M. Matsuo, Y. Serizawa, and K. Mizuyama, Nucl. Phys. **A788**, 307c (2007).
- [14] E. Khan, N. Sandulescu, M. Grasso, and N. V. Giai, Phys. Rev. C **66**, 024309 (2002).
- [15] E. Khan, N. Sandulescu, N. V. Giai, and M. Grasso,

- Phys. Rev. C **69**, 014314 (2004).
- [16] E. Khan, N. Sandulescu, and N. V. Giai, Phys. Rev. C **71**, 042801 (2005).
- [17] S. Goriely and E. Khan, Nucl. Phys. **A706**, 217 (2002).
- [18] N. Paar, P. Ring, T. Nikšić, and D. Vretenar, Phys. Rev. C **67**, 034312 (2003).
- [19] N. Paar, T. Nikšić, D. Vretenar, and P. Ring, Phys. Rev. C **69**, 054303 (2004).
- [20] M. Yamagami and N. V. Giai, Phys. Rev. C **69**, 034301 (2004).
- [21] M. Yamagami, E. Khan, and N. V. Giai, in *Proceedings of the International Symposium on Frontiers Of Collective Motions(CM2002)* (World Scientific, Singapore, 2002), pp. 230–235, edited by H. Sagawa and H. Iwasaki.
- [22] M. Yamagami, Phys. Rev. C **72**, 064308 (2005).
- [23] J. Terasaki, J. Engel, M. Bender, J. Dobaczewski, W. Nazarewicz, and M. Stoitsov, Phys. Rev. C **71**, 034310 (2005).
- [24] J. Terasaki and J. Engel, Phys. Rev. C **74**, 044301 (2006).
- [25] K. Yoshida, M. Yamagami, and K. Matsuyanagi, Nucl. Phys. **A779**, 99 (2006).
- [26] N. Paar, D. Vretenar, E. Khan, and G. Colo, Rep. Prog. Phys. **70**, 691 (2007).
- [27] S. O. Bäckman, A. D. Jackson, and J. Speth, Phys. Lett. **56B**, 209 (1975).
- [28] N. V. Giai and H. Sagawa, Phys. Lett. **106B**, 379 (1981).
- [29] P. Bonche, H. Flocard, and P. H. Heenen, Nucl. Phys. **A467**, 115 (1986).
- [30] M. Bender, P. H. Heenen, and P. G. Reinhard, Rev. Mod. Phys. **75**, 121 (2003).
- [31] M. Beiner, H. Flocard, N. V. Giai, and P. Quentin, Nucl. Phys. **A238**, 29 (1975).
- [32] J. Bartel, P. Quentin, M. Brack, C. Guet, and H. B. Hakansson, Nucl. Phys. **A386**, 79 (1982).
- [33] E. Chabanat, P. Bonche, P. Haensel, J. Meyer, and F. Schaeffer, Nucl. Phys. **A635**, 231 (1998).
- [34] G. F. Bertsch and H. Esbensen, Ann. Phys. **209**, 327 (1991).
- [35] J. Dobaczewski, W. Nazarewicz, and P. G. Reinhard, Nucl. Phys. **A693**, 361 (2001).
- [36] G. F. Bertsch and S. F. Tsai, Phys. Rep. **18**, 125 (1975).
- [37] F. E. Serr, T. S. Dumitrescu, T. Suzuki, and C. H. Dasso, Nucl. Phys. **A404**, 359 (1983).
- [38] A. Bohr and B. R. Motterson, *Nuclear Structure*, Vol. 2. (Benjamin, New York, 1998).
- [39] E. Lipparini and S. Stringari, Phys. Rep. **175**, 103 (1989).
- [40] K. F. Liu and N. V. Giai, Phys. Lett. **65B**, 23 (1976).
- [41] I. Hamamoto, H. Sagawa, and X. Z. Zhang, Phys. Rev. C **55**, 2361 (1997).
- [42] I. Hamamoto, H. Sagawa, and X. Z. Zhang, Nucl. Phys. **A648**, 203 (1999).
- [43] H. Sagawa, Prog. Theor. Phys. Suppl. **142**, 1 (2001).
- [44] S. T. Belyaev, A. V. Smirnov, S. V. Tolokonnikov, and S. A. Fayans, Sov. J. Nucl. Phys. **45**, 783 (1987).
- [45] W. Satuła, J. Dobaczewski, and W. Nazarewicz, Phys. Rev. Lett. **81**, 3599 (1998).
- [46] S. Shlomo and G. Bertsch, Nucl. Phys. **A676**, 49 (1975).
- [47] A. Leistenschneider, T. Aumann, K. Boretzky, D. Cortina, J. Cub, U. D. Pramanik, W. Dostal, T. W. Elze, H. Emling, H. Geissel, *et al.*, Phys. Rev. Lett. **86**, 5442 (2001).
- [48] P. G. Thirolf, B. V. Pritychenko, B. A. Brown, P. D. Cottle, M. Chromik, T. Glasmacher, G. Hackman, R. W. Ibbotson, K. W. Kemper, T. Otsuka, *et al.*, Phys. Lett. B **485**, 16 (2000).
- [49] *Electric and Magnetic Giant Resonances in Nuclei*, edited by J. Speth (World Scientific, Singapore, 1991).
- [50] M. N. Harakeh and A. V. D. Woude, *Giant Resonances: Fundamental High-Frequency Modes of Nuclear Excitation* (Oxford University Press, New York, 2001).
- [51] T. Sil, S. Shlomo, B. K. Agrawal, and P. G. Reinhard, Phys. Rev. C **73**, 034316 (2006).
- [52] M. Matsuo, Phys. Rev. C. **73**, 044309 (2006).
- [53] F. Catara, E. G. Lanza, M. A. Nagarajan, and A. Vitturi, Nucl. Phys. **A624**, 449 (1997).
- [54] D. Vretenar, N. Paar, P. Ring, and G. A. Lalazissis, Nucl. Phys. **A692**, 496 (2001).